Mon. Not. R. Astron. Soc. **314**, 713–726 (2000)

# Spatially resolved spectra of the accretion disc of the nova-like variable UU Aquarii

Raymundo Baptista,[1★] C. Silveira,[1★] J. E. Steiner[2★] and Keith Horne[3★]

[1]*Departamento de Física, Universidade Federal de Santa Catarina, Campus Trindade, 88040-900, Florianópolis – SC, Brazil*
[2]*Laboratório Nacional de Astrofísica–LNA/CNPq, CP 21, 37500-000, Itajubá, Brazil*
[3]*School of Physics & Astronomy, University of St Andrews, North Haugh, St Andrews, Fife KY16 9SS*

Accepted 1999 November 30. Received 1999 November 23; in original form 1999 September 21



**ABSTRACT**

Time-resolved spectroscopy of the nova-like variable UU Aquarii is analysed with eclipse mapping techniques to produce spatially resolved spectra of its accretion disc and gas stream as a function of distance from disc centre in the range 3600–6900 Å. The spatially resolved spectra show that the continuum emission becomes progressively fainter and redder for increasing disc radius – reflecting the radial temperature gradient – and reveal that the H I and He I lines appear as deep, narrow absorption features in the inner disc regions, transitioning to emission with P Cyg profiles for intermediate and large disc radii. The spectrum of the uneclipsed component has strong H I and He I emission lines plus a Balmer jump in emission, and is explained as optically thin emission from a vertically extended disc chromosphere + wind. Most of the line emission probably arises from the wind. The spatially resolved spectra also suggest the existence of gas stream 'disc-skimming' overflow in UU Aqr, which can be seen down to $R \simeq 0.2R_{\rm L1}$. The comparison of our eclipse maps with those of Baptista, Steiner & Horne suggests that the asymmetric structure in the outer disc previously identified as the bright-spot may be the signature of an elliptical disc similar to those possibly present in SU UMa stars during superoutbursts.

**Key words:** accretion, accretion discs – binaries: close – binaries: eclipsing – stars: individual: UU Aqr – novae, cataclysmic variables.

## 1 INTRODUCTION

The standard picture of a nova-like system is that of a close binary in which a late-type star fills its Roche lobe and transfers matter to a companion white dwarf via an accretion disc. A bright-spot is expected to form where the gas stream from the donor star hits the edge of the accretion disc.

The SW Sex stars (Thorstensen et al. 1991) form a sub-class of the nova-likes with orbital periods in the range 3–4 h that do not seem to fit within the above standard picture, displaying a range of peculiarities: (i) single-peaked asymmetric emission lines showing little eclipse; (ii) large (~70°) phase shifts between photometric and spectroscopic conjunction; (iii) orbital phase-dependent absorption in the Balmer lines; (iv) Doppler tomograms bright in the lower left quadrant with small or no sign of disc emission; and (v) V-shaped continuum eclipses implying flat radial temperature profiles in the inner disc (e.g. Warner 1995 and references therein). Earlier proposals to explain the phenomenon include accretion disc winds (Honeycutt, Schlegel & Kaitchuck 1986), magnetic white dwarfs disrupting the inner disc (Williams 1989), and gas stream overflow (Hellier & Robinson 1994). The two most recent models proposed to explain the phenomenology of the SW Sex stars are the disc-anchored magnetic propeller (Horne 1999) and a combination of stream overflow + disc winds (Hellier 2000).

UU Aqr is an eclipsing nova-like ($P_{\rm orb} = 3.9$ h) with a spectrum that is dominated by single-peaked strong Balmer and He I emission lines (e.g. Downes & Keyes 1988). H$\alpha$ spectroscopy has revealed that the line profile is highly asymmetric and phase-dependent, and that the spectroscopic conjunction lags mid-eclipse by ~0.15 cycle (Haefner 1989; Diaz & Steiner 1991). The lack of the rotational disturbance typical of emitting accretion discs during eclipse in H$\beta$ led Hessman (1990) to the suggestion that the emission lines have a non-disc origin.

Baptista, Steiner & Cieslinski (1994, hereafter BSC94) derived a photometric model for the binary with a mass ratio $q = 0.30$, a primary mass $M_1 = 0.67\,{\rm M}_\odot$ and an inclination of $i = 78°$. From the analysis of mid-eclipse fluxes, they suggested that the Balmer lines are formed in an extended region only partially occulted during eclipse, possibly in a wind emanating from the inner disc. They also found that UU Aqr presents long-term brightness variations of low amplitude (≃0.3 mag) on time-scales of years.

★ E-mail: bap@fsc.ufsc.br (RB); silveira@fsc.ufsc.br (CS); steiner@lna.br (JES); kdh1@st-and.ac.uk (KH)

**Table 1.** Journal of the observations.

| Date (1993) | Run | UT start | UT end | No. of spectra | Spectral range (Å) | Cycle number | Phase range (cycle) |
|---|---|---|---|---|---|---|---|
| 22 July | 1 | 05:56 | 07:33 | 105 | 3564.0–6766.5 | 17389 | −0.20, +0.21 |
| 27 July | 2 | 07:59 | 09:40 | 111 | 3601.6–6805.5 | 17420 | −0.11, +0.32 |
| 13 August | 3 | 07:52 | 09:25 | 101 | 3646.5–6850.5 | 17524 | −0.22, +0.17 |
| 15 August | 4 | 07:01 | 08:37 | 106 | 3649.5–6853.5 | 17536 | −0.20, +0.20 |
| 16 August | 5 | 06:18 | 08:18 | 110 | 3649.5–6853.5 | 17542 | −0.27, +0.24 |

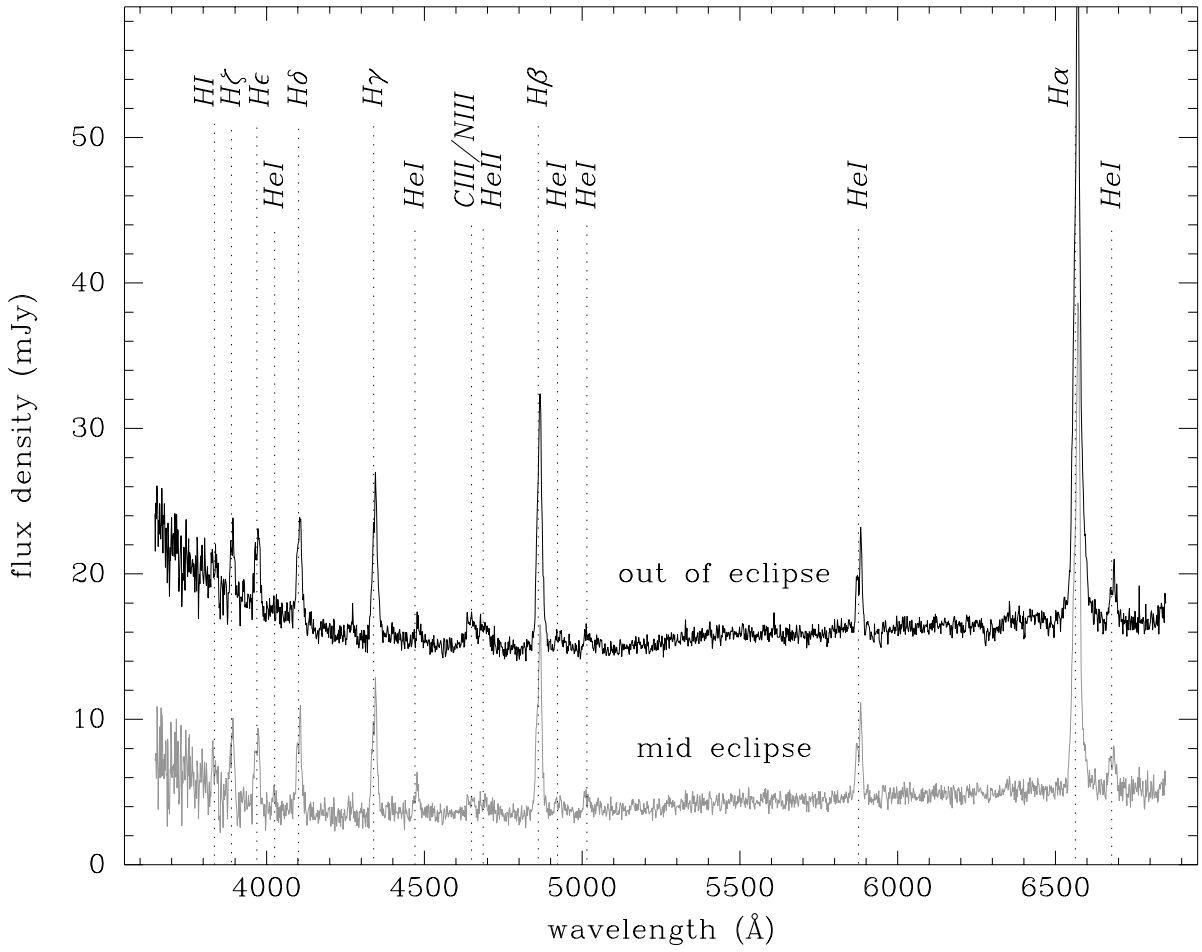


**Figure 1.** Average out-of-eclipse (upper spectrum, phase range −0.22 to −0.06 cycle) and mid-eclipse (lower spectrum, phase range −0.025 to 0.025 cycle) spectra of UU Aqr on 1995 August 13. Major emission features are indicated by vertical dotted lines.

The eclipse mapping study of Baptista, Steiner & Horne (1996, hereafter BSH96) indicates that the inner disc of UU Aqr is optically thick, resulting in a distance estimate of 200 pc. Temperatures in the disc range from ∼6000 K in the outer regions to ∼16 000 K near the white dwarf at disc centre. The radial temperature profiles in the high state follow the $T \propto R^{-3/4}$ law in the outer and intermediate disc regions, but flatten off in the inner disc, leading to mass accretion rates of $\dot{M} = 10^{-9.2}\,\mathrm{M}_\odot\,\mathrm{yr}^{-1}$ at $R = 0.1R_{\mathrm{L1}}$ and $\dot{M} = 10^{-8.8}\,\mathrm{M}_\odot\,\mathrm{yr}^{-1}$ at $R = 0.3R_{\mathrm{L1}}$ ($R_{\mathrm{L1}}$ is the distance from disc centre to the inner Lagrangian point). Together with other characteristics, this led BSH96 to suggest that UU Aqr was an SW Sex star. The comparison of eclipse maps of the low and high states revealed that the differences are due to changes in the structure of the outer parts of the disc, the most noticeable effect being the appearance of a conspicuous red, bright structure at disc rim, which the authors identified with the bright-spot.

According to BSH96, the mass accretion rate of UU Aqr is barely above the critical limit for disc instability to set in. Warner (1997) noted that the outer disc temperature is only 6000 K, and remarked that small variations in $\dot{M}$ could led to dwarf nova type outbursts. Honeycutt, Robertson & Turner (1998) performed a long-term photometric monitoring of UU Aqr which confirmed the high- and low-brightness states of BSC94, and revealed the existence of small-amplitude (≲1.0 mag) brightness variations on time-scales of a few days, which they called 'stunted outbursts'.

The detailed spectroscopic study of Hoard et al. (1998) reinforced the classification of UU Aqr as an SW Sex star. They found evidence for the presence of a bright-spot at the impact site of the gas stream with the edge of the disc, and a

non-axisymmetric, vertically and azimuthally extended absorbing structure in the disc. They proposed an explanation for the absorbing structure, as well as for the other spectroscopic features of UU Aqr, in terms of the explosive impact of the accretion stream with the disc. Optical and ultraviolet spectroscopy by Kaitchuck et al. (1998) shows a secondary eclipse at phase 0.4 in the optical and Balmer lines (but not in the ultraviolet continuum or lines), which they suggested may be caused by an occultation of the bright-spot and stream region by material suspended above the inner disc.

In this paper we report on the analysis of time-resolved spectroscopy of UU Aqr with multiwavelength eclipse mapping techniques to derive spatially resolved spectra of the accretion flow in this binary. Section 2 describes the observations and data reduction procedures, while Section 3 describes the analysis of the light curves with eclipse mapping techniques. Section 4 presents eclipse maps at selected wavelengths, the radial intensity and brightness temperature distributions, and spatially resolved spectra of the accretion disc and gas stream, as well as the spectrum of the uneclipsed component. The results are discussed in Section 5 and summarized in Section 6.

## 2 OBSERVATIONS

Time-resolved spectroscopy covering five eclipses of UU Aqr was obtained with the 2.1-m telescope at the Kitt Peak National Observatory (KPNO) in 1993 July–August in the spectral range 3500–6900 Å (spectral resolution $\Delta\lambda = 1.5$ Å pixel$^{-1}$). The observations consist of five sets of $\simeq$100 short-exposure ($\Delta t = 30$ s) spectra at a time resolution of 50 s. A close comparison star (star C1 of BSC94) was included in the slit to allow correction of sky transparency variations and slit losses. The observations (summarized in Table 1) were performed under good (cloud-free) sky conditions and at small to moderate airmasses ($X \leq 1.4$) except for run 1, which started while the object was still at a reasonably high zenith angle ($X = 2.2$).

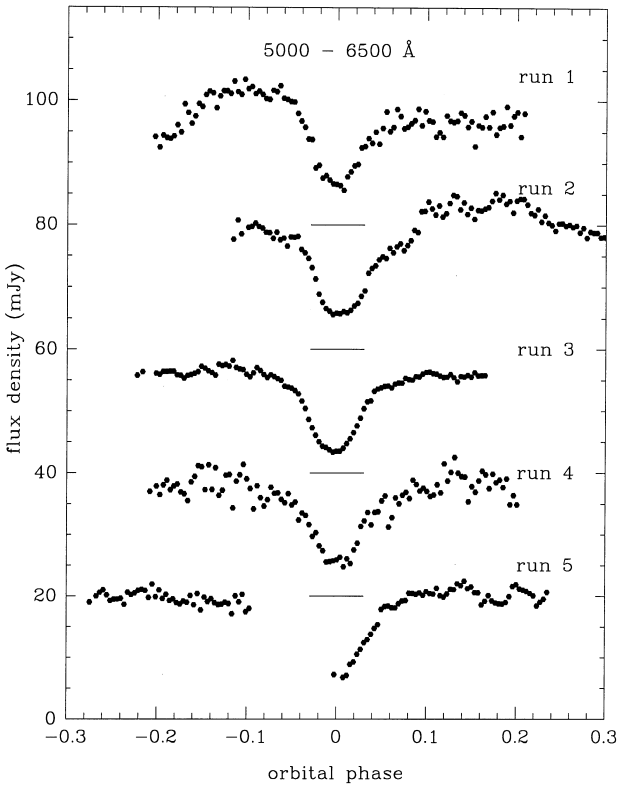


**Figure 2.** Broad-band light curves of the UU Aqr data set. The curves are progressively displaced upwards by 20 mJy for visualization purposes. Horizontal lines at mid-eclipse show the true zero level in each case.

The data were bias-subtracted and corrected for flat-field and slit illumination effects using standard IRAF procedures. One-dimensional spectra of both variable and comparison star were extracted with the optimal extraction algorithm of Horne (1986). The individual spectra were checked for the presence of possible cosmic rays and, when appropriate, were corrected by interpolation from the neighbouring wavelengths. Arc-lamp observations were used to calibrate the wavelength scale (with an accuracy of 0.15 Å). Observations of the standard spectrophotometric stars BD+28 4211 and G191 B2B (Massey et al. 1988) were used to derive the instrumental sensitivity function and to flux-calibrate the set of extracted spectra on each night. Error bars were computed taking into account the photon count noise and the sensitivity response of the instrument.

The reduced spectra were combined to produce trailed spectrograms of the variable and the comparison star for each night. The display of the trailed spectrograms of the comparison stars shows that there were non-negligible sky transparency variations and/or time-dependent slit losses along the runs. We defined a reference spectrum of the comparison star by computing an average of 40 spectra on night 5, corresponding to the time for which the star was closest to zenith. We normalized the spectrograms of the comparison star by dividing each spectrum by the reference spectrum. A two-dimensional cubic spline fit was used to produce a smoothed version of the normalized spectrograms. The sky transparency variations and variable slit losses were corrected by dividing the spectrogram of the variable by the smoothed, normalized spectrogram of the comparison star on each night (a procedure analogous to the flat-field correction). The reference spectrum is consistent with the *UBVRI* photometry of star C1 (BSC94) at the $1\sigma$ level. The absolute photometric accuracy of these observations should therefore be better than 10 per cent.

Fig. 1 shows average out-of-eclipse and mid-eclipse spectra of UU Aqr on 1995 August 13. The spectra are dominated by strong single-peaked Balmer emission lines, but also show He I lines and the blend of C III, N III and He II lines at ~4650 Å. The emission lines have asymmetrical shapes, the red side of the line being stronger, in accordance with the results of Hessman (1990) and Diaz & Steiner (1991). The He I lines and the higher energy Balmer lines show a possible double-peaked structure, suggesting either classical double-peaked emission from a highly inclined disc or single-peaked emission with a central absorption component. While the continuum is reduced by a factor of $\simeq$3 during eclipse, the emission lines suffer a much smaller reduction in flux, suggesting that they possibly arise from a vertically extended source that is larger than the accretion disc (responsible for the continuum emission), in accordance with inferences drawn by BSC94.

Fig. 2 shows light curves of the five runs in the broad band 5000–6500 Å. The gap in run 5 is due to an interruption of the observations to check the telescope focus. The light curves have similar eclipse shapes and out-of-eclipse flux levels, with variations at the level of $\lesssim$20 per cent between the runs. Indications that the observations were performed while UU Aqr was in its high-brightness state come from the eclipse shape and average out-of-eclipse flux level. The latter suggests that

the object was even slightly brighter than the typical high-brightness state of BSC94. These remarks are in agreement with the historical light curve of Honeycutt et al. (1998, see their fig. 1), which shows that UU Aqr reached a maximum of its long-term average brightness level during 1993, the epoch of our observations. The spectral range of the light curves in Fig. 1 corresponds roughly to the $V$ band. The average out-of-eclipse level of all runs yields an approximate mean magnitude of $V = 13.2 \pm 0.2$ mag, consistent with the value drawn from the light curve of Honeycutt et al. (1998), of $V = 13.4 \pm 0.6$ mag.

## 3 DATA ANALYSIS

### 3.1 Light curve construction

The spectra were divided into 226 passbands of 15 Å in the continuum and fainter lines, and $\simeq 500\,\mathrm{km\,s^{-1}}$ across the most prominent lines. For each passband a light curve was extracted by computing the average flux over the corresponding wavelength range and phase-folding the resulting data according to the ephemeris of BSC94. A phase correction of $-0.003$ cycle was further applied to the data to make the centre of the white dwarf

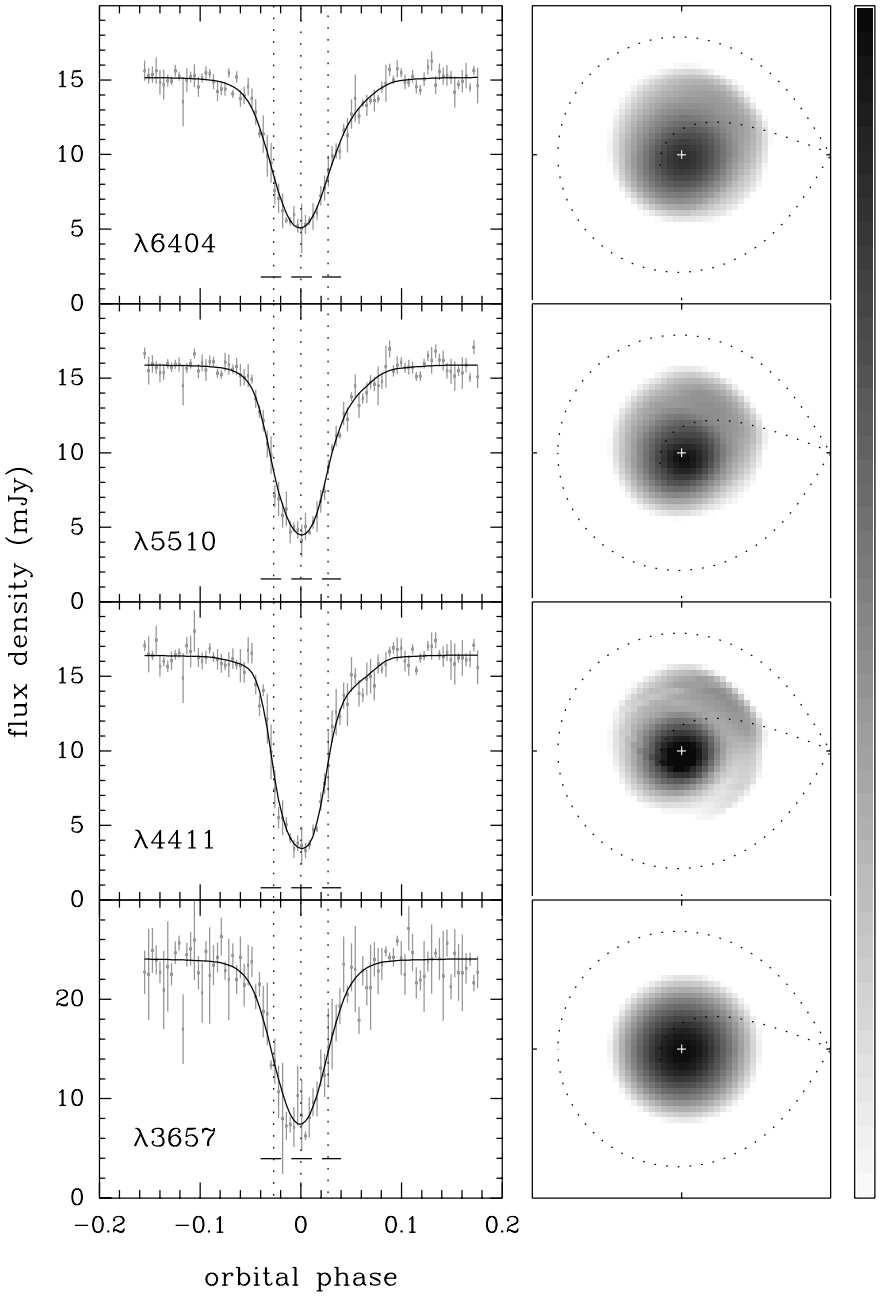


**Figure 3.** Light curves (left) and eclipse maps (right) at selected continuum passbands. Data light curves are shown as data points with error bars, and the fitted models appear as solid curves. A horizontal dashed line depicts the uneclipsed component in each case. Labels indicate the central wavelength of each passband. Eclipse maps are shown to the right in a logarithmic grey-scale: dark regions are brighter; white corresponds to $\log I_\nu = -6.5$, and black to $\log I_\nu = -3.1$. Dotted curves show the projection of the primary Roche lobe on to the orbital plane and the theoretical gas stream trajectory; the secondary star is to the right of each panel and the stars rotate counter-clockwise.

eclipse coincident with phase zero. For those passbands including emission lines, the light curves comprise the total flux at the corresponding bin with no subtraction of a possible underlying continuum contribution.

Since all the observations in the data set correspond to the same brightness level, it was possible to combine the light curves of all runs to produce average light curves for each passband. This helps to increase the signal-to-noise ratio of the light curves and to reduce the influence of flickering in the eclipse shape. For each passband, we first normalized the individual light curves by fitting a spline function to the phases outside eclipse and dividing the light curve by the fitted spline. The normalized light curves were combined by separating the data into phase bins of 0.0038 cycle and computing the median for each bin. The median of the absolute deviations with respect to the median for each bin is taken as the corresponding uncertainty. The resulting light curve is scaled back to flux units by multiplying the combined light curve by the median flux of the spline functions at phase zero. This procedure removes orbital variations outside eclipse with only minor effects on the eclipse shape itself.

### 3.2 Eclipse mapping

The eclipse mapping method was used to solve for a map of the disc brightness distribution and for the flux of an additional uneclipsed component in each passband. For the details of the

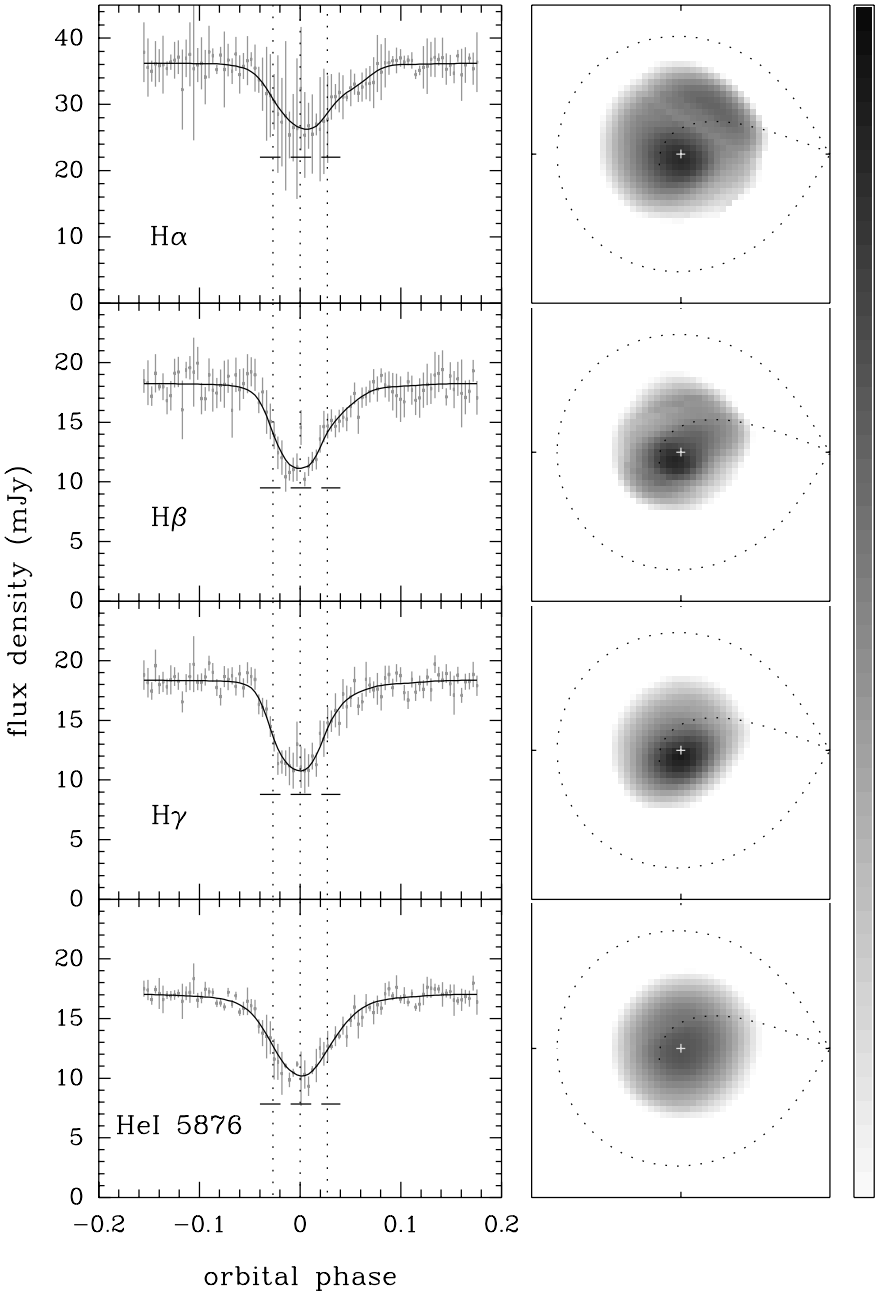


**Figure 4.** Light curves (left) and eclipse maps (right) for the H$\alpha$, H$\beta$, H$\gamma$ and He I $\lambda$5876 line centre passbands. The notation and logarithmic grey-scale are the same as in Fig. 3.

method the reader is referred to Horne (1985, 1993), Baptista & Steiner (1993) and Rutten et al. (1994).

For our analysis we adopted the same eclipse map as BSH96, a $51 \times 51$ pixel grid centred on the primary star with side $2R_{\rm L1}$, where $R_{\rm L1}$ is the distance from the disc centre to the inner Lagrangian point. This choice provides maps with a nominal spatial resolution of $0.039R_{\rm L1}$, comparable to the expected size of the white dwarf in UU Aqr ($\simeq 0.032R_{\rm L1}$). The eclipse geometry is specified by the mass ratio $q$ and the inclination $i$. We adopted the parameters of BSC94, $i = 78^\circ$ and $q = 0.3$. The specific intensities in the eclipse map were computed assuming $R_{\rm L1} = 0.74\,{\rm R}_\odot$ (BSC94) and a distance of 200 pc (BSH96).

The statistical uncertainties of the eclipse maps were estimated with a Monte Carlo procedure (e.g. Rutten, van Paradijs & Tinbergen 1992; Baptista et al. 1995). For a given narrow-band light curve, a set of 10 artificial light curves is generated, in which the data points are independently and randomly varied according to a Gaussian distribution with standard deviation equal to the uncertainty at that point. The light curves are fitted with the eclipse mapping algorithm to produce a set of randomized eclipse maps. These are combined to produce an average map and a map of the residuals with respect to the average, which yields the statistical uncertainty at each pixel. The uncertainties obtained with this procedure are used when estimating the errors in the derived radial temperature and intensity profiles, as well as in the spatially resolved spectra.

Average light curves, fitted models and eclipse maps at selected passbands are shown in Figs 3 and 4. These will be discussed in detail in Section 4.

## 4 RESULTS

### 4.1 Accretion disc structure

In this section we compare eclipse maps at selected passbands in order to study the structure of the accretion disc at different wavelengths.

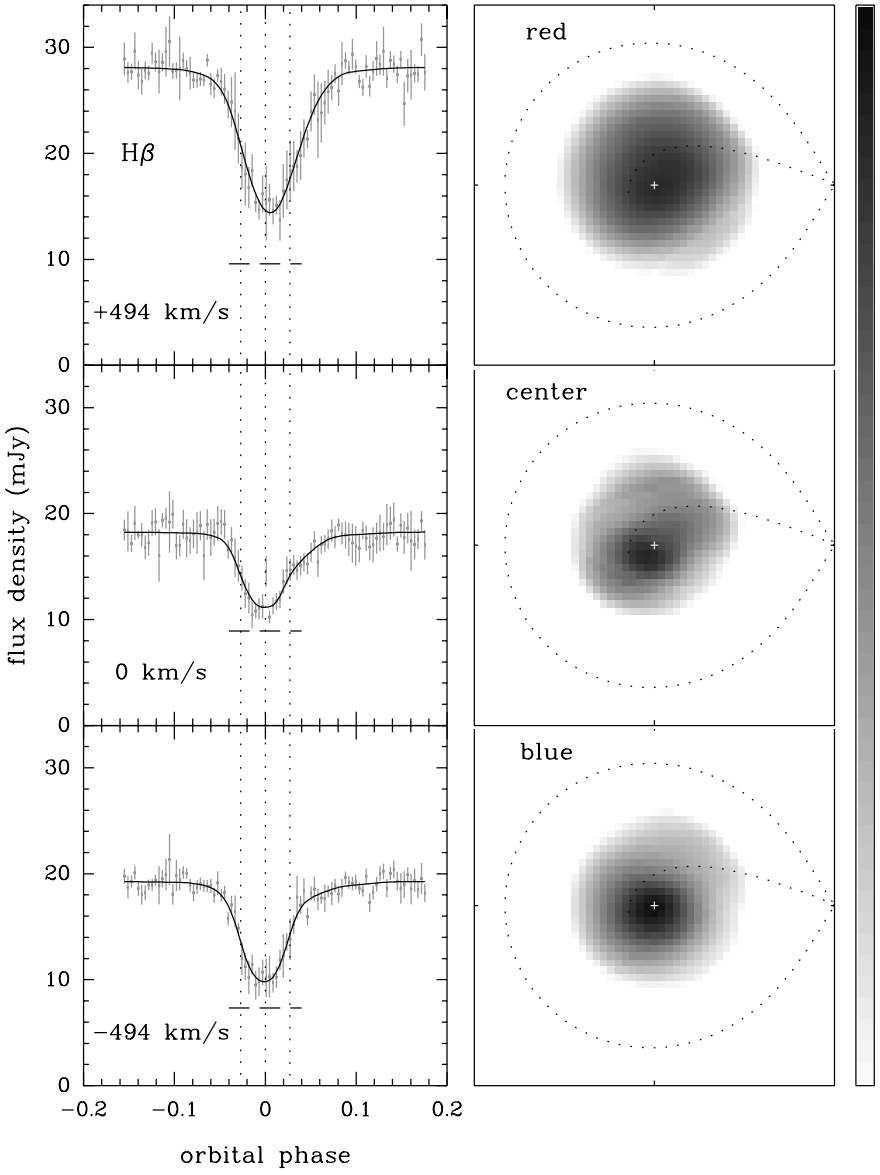


**Figure 5.** H$\beta$ velocity-resolved light curves (left) and eclipse maps (right) at velocities of $-494$, 0 and $+499\,{\rm km\,s^{-1}}$. The notation and logarithmic grey-scale are the same as in Fig. 3.

Fig. 3 shows light curves (left-hand panels) and eclipse maps (right-hand panels) of four selected continuum passbands close to the Johnson–Cousins *UBVR* effective wavelengths in order to allow a comparison with the results of BSH96. Horizontal dashed lines depict the uneclipsed component in each case. The continuum light curves show a deep eclipse with a slightly asymmetric egress shoulder which is more pronounced for longer wavelengths. This results in eclipse maps with brightness distributions concentrated towards disc centre, and asymmetric structures in the trailing quadrant of the disc closest to the secondary star (the upper right quadrant in the eclipse maps of Fig. 3). The uneclipsed component at $\lambda 3657$ is perceptibly larger than at $\lambda 4411$, suggesting that the Balmer jump is in emission and that the uneclipsed light has an important contribution from optically thin gas. This is in line with previous results by BSC94 and BSH96. The eclipse shapes and out-of-eclipse levels resemble those of the high-brightness state observed by BSH96, although with a less pronounced asymmetry at eclipse egress. Accordingly, the eclipse maps clearly lack the noticeable asymmetric structure at disc edge which was the main characteristic of the high state (BSH96, see their fig. 3). We will return to this point in Section 5.

Fig. 4 shows light curves and eclipse maps for the line centre passbands of H$\alpha$, H$\beta$, H$\gamma$ and He I $\lambda 5876$. We remark that the line light curves include the total flux at the corresponding wavelength range, with no subtraction of an interpolated continuum. The eclipses are shallow, leading to brightness distributions that are flatter than those of the continuum. Similar to the continuum maps, the asymmetry in the egress shoulder is more pronounced for the lines at longer wavelengths. The uneclipsed components are considerably larger than in the continuum, indicating that the uneclipsed spectrum has strong Balmer and He I emission lines. The large error bars of the H$\alpha$ centre light curve are due not to low signal-to-noise ratio but to the variability of the eclipse shape at this wavelength. This effect is also seen, although to a lesser extent, in H$\beta$ and H$\gamma$.

Fig. 5 shows (Doppler) velocity-resolved light curves (left) and eclipse maps (right) across the H$\beta$ line. There is marginal evidence of rotational disturbance: the minimum of the blue bin light curve ($-494\,\mathrm{km\,s^{-1}}$) is slightly displaced towards negative phases, while that of the red bin light curve ($+494\,\mathrm{km\,s^{-1}}$) is correspondingly displaced towards positive phases, suggesting that the line-emitting gas rotates in the prograde sense. However, the eclipse maps in the symmetric velocity bins do not show the mirror symmetry (over the line joining both stars) expected for line emission from a Keplerian disc around the white dwarf. Equally remarkable are the facts that the light curve in the red bin has a much larger out-of-eclipse flux than its blue counterpart, and that the corresponding eclipse map is perceptibly brighter than that of the blue bin anywhere. A similar behaviour is found in the other lines for which velocity-resolved maps were obtained. This cannot be attributed to the underlying continuum, since the interpolated continuum has essentially a constant level across each line. It seems clear that most of the line emission does not arise from a disc in Keplerian rotation.

### 4.2 Radial temperature distribution and mass accretion rate estimate

The simplest way of testing theoretical disc models is to convert the intensities in the eclipse maps to blackbody brightness temperatures, which can then be compared with the radial run of the effective temperature predicted by steady-state, optically thick disc models. However, as discussed by Baptista et al. (1998),

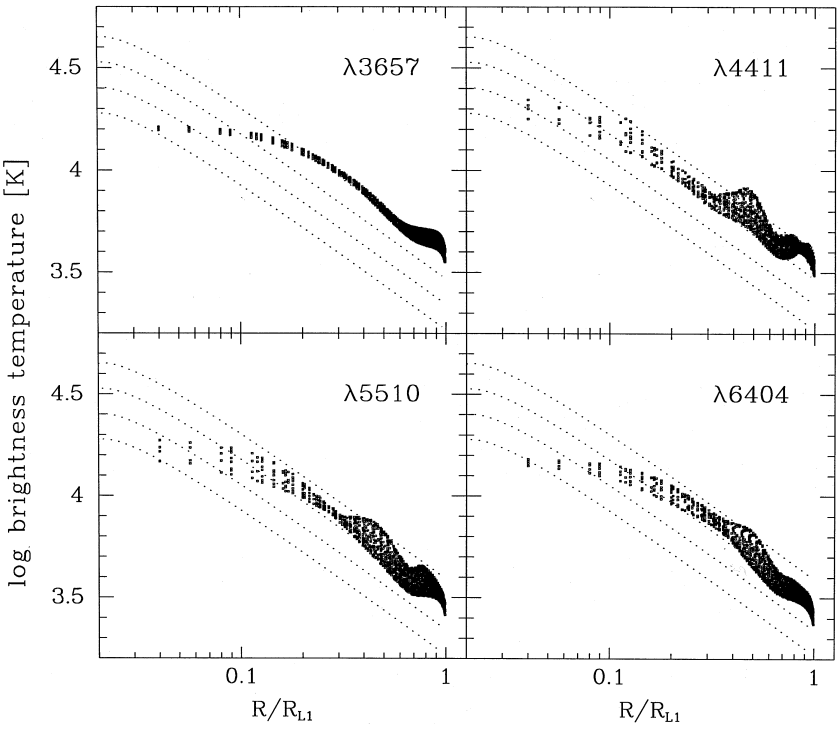


**Figure 6.** Brightness temperature radial distributions of the UU Aqr accretion disc for the continuum maps of Fig. 3, calculated assuming a distance of 200 pc to the system (BSH96). Dotted lines correspond to steady-state disc models for mass accretion rates of $\dot{M} = 10^{-8.5}$, $10^{-9}$, $10^{-9.5}$ and $10^{-10}\,\mathrm{M_\odot\,yr^{-1}}$, assuming $M_1 = 0.67\,\mathrm{M_\odot}$ and $R_1 = 0.012\,\mathrm{R_\odot}$ (BSC94). Abscissae are in units of the distance from disc centre to the inner Lagrangian point ($R_{L1}$).

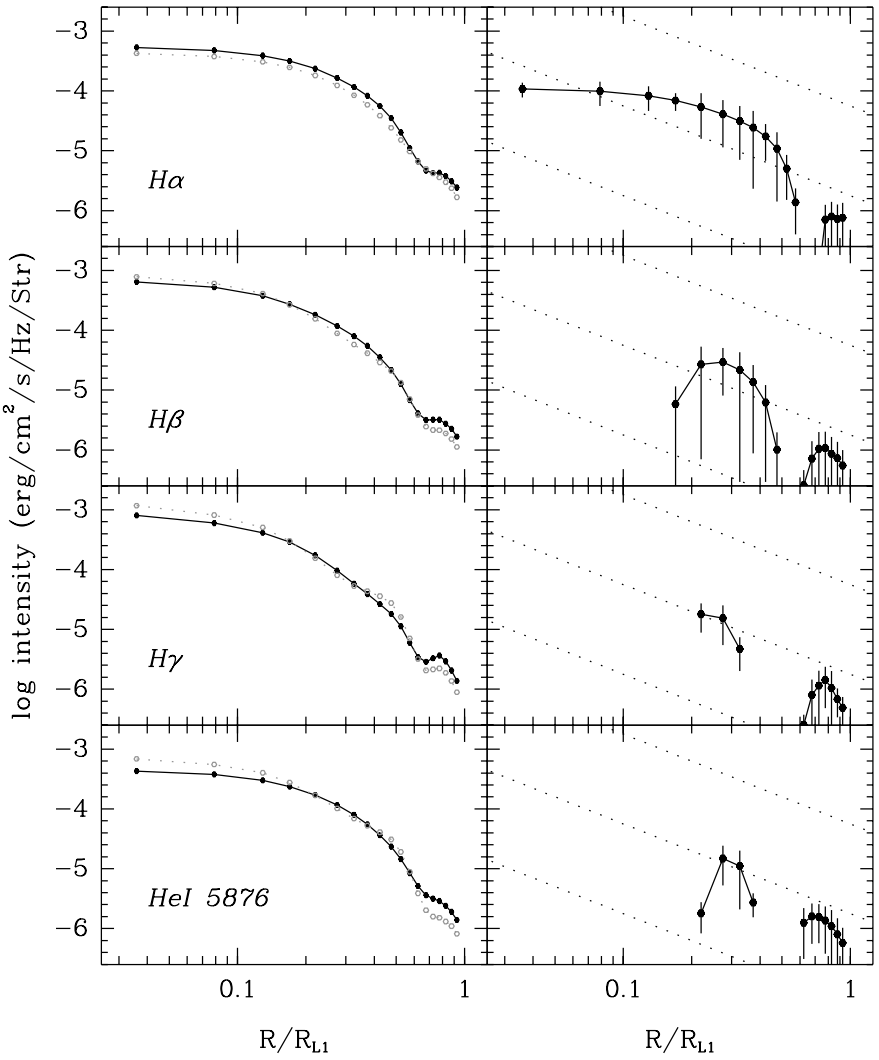


**Figure 7.** Left-hand panels: radial line intensity profiles for the most prominent lines (solid) and adjacent continuum (dotted), calculated assuming a distance of 200 pc to the system (BSH96). Abscissae are in units of the distance from disc centre to the inner Lagrangian point ($R_{\rm L1}$). Right-hand panels: the net line emission radial distributions. Dotted lines depict the slope of the expected relation $I \propto R^{-1.5}$.

a relation between the effective temperature and a monochromatic brightness temperature is non-trivial, and can only be properly obtained by constructing self-consistent models of the vertical structure of the disc. Therefore our analysis here is meant as preliminary, and should be complemented by detailed disc spectrum modelling in a future paper.

Fig. 6 shows brightness temperature radial distributions for the continuum maps of Fig. 3 in a logarithmic scale. Each temperature shown is the blackbody brightness temperature that reproduces the observed surface brightness at the corresponding pixel assuming a distance of 200 pc to UU Aqr (BSH96). Steady-state disc models for mass accretion rates of $10^{-8.5}$, $10^{-9}$, $10^{-9.5}$ and $10^{-10}\,{\rm M}_\odot\,{\rm yr}^{-1}$ are plotted as dotted lines for comparison. These models assume that $M_1 = 0.67\,{\rm M}_\odot$ and $R_1 = 0.012\,{\rm R}_\odot$ (BSC94).

The distributions resemble those obtained by BSH96 for the high-brightness state of UU Aqr, closely following the $T \propto R^{-3/4}$ law for steady accretion in the intermediate and outer disc regions ($R \geq 0.2R_{\rm L1}$), but displaying a noticeable flattening in the inner disc ($R < 0.1R_{\rm L1}$). Temperatures range from $\sim$18 000 K in the inner disc to 6000 K in the outer disc regions, leading to inferred mass accretion rates of $\dot{M} = 10^{-9.0\pm0.3}\,{\rm M}_\odot\,{\rm yr}^{-1}$ at $R = 0.1R_{\rm L1}$ and $10^{-8.7\pm0.2}\,{\rm M}_\odot\,{\rm yr}^{-1}$ at $R = 0.3R_{\rm L1}$ – in good agreement with the results of BSH96 for the high-brightness state. The quoted errors on $\dot{M}$ account for the statistical uncertainties in the eclipse maps, obtained from the Monte Carlo procedure described in Section 3.2, and the scatter in the temperatures of maps at different wavelengths. The eclipse map at $\lambda$3657 leads to temperatures that are systematically higher than those of the other continuum maps of Fig. 3, in an example of the limitations of using brightness temperatures to estimate the mass accretion rate. This difference reflects the fact that the Balmer jump appears in emission for the intermediate and outer disc regions, as will be seen in Section 4.4.

### 4.3 Radial line intensity distributions

The left-hand panels in Fig. 7 show radial intensity distributions for the most prominent lines (solid) and adjacent continuum (dotted) on a logarithmic scale. The line distributions were obtained from the average of all eclipse maps across the line region, while the continuum distributions were obtained from the average of eclipse maps on both sides of each line. Net line

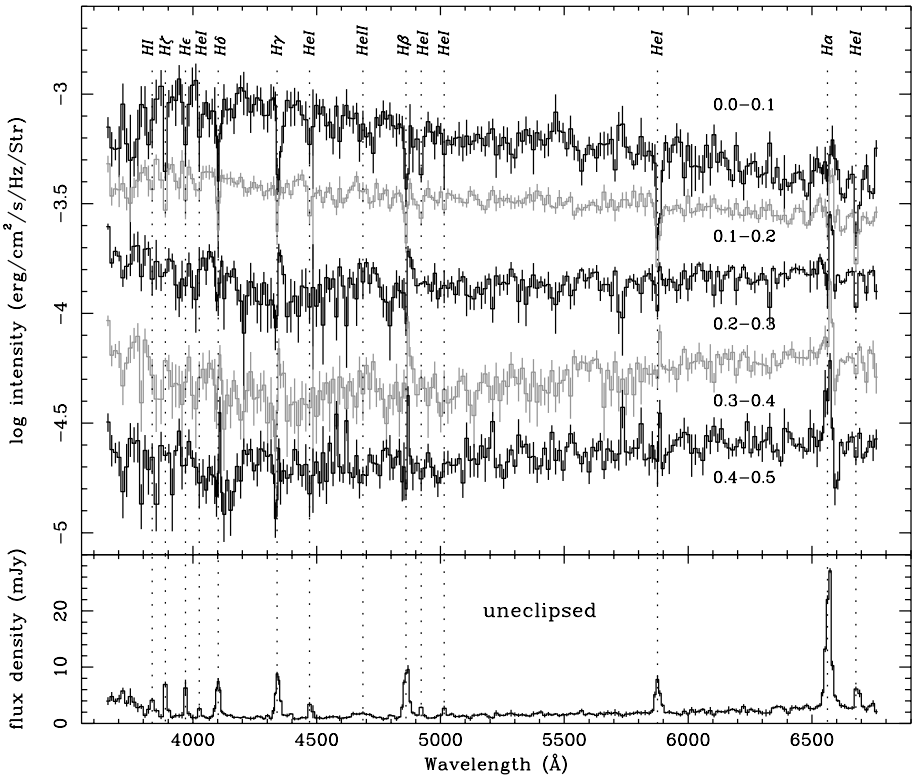


**Figure 8.** Spatially resolved spectra of the UU Aqr accretion disc. The spectra were computed for a set of concentric annular sections (radius range indicated on the right, in units of $R_{L1}$). The lower panel shows the spectrum of the uneclipsed light. The most prominent line transitions are indicated by vertical dotted lines. Error bars were derived via Monte Carlo simulations with the eclipse light curves.

emission distributions were computed by subtracting the distributions of the adjacent continuum from those of the lines, and are shown in the right-hand panels. In the external map regions ($R \gtrsim 0.7R_{L1}$) the intensities of both line and continuum drop by a factor of $\sim 10^3$ with respect to the inner disc regions, making the computation of the net emission quite noisy and unreliable. H$\alpha$ is seen in emission (intensities larger than those at the adjacent continuum) at all disc radii and up to $R \simeq 0.6R_{L1}$. The other lines are in absorption in the inner disc and transition to emission at intermediate ($R \sim 0.2R_{L1}$) disc radius. This behaviour is noticeably different from that observed in the low-brightness state, where H$\alpha$ is seen in emission in the inner disc and disappears into the continuum for $R \simeq 0.3R_{L1}$ (BSH96). This result suggests that the line emission region increases in size from the low- to the high-brightness state, possibly in response to changes in mass accretion rate. The transition from absorption to emission occurs at larger disc radii for lines of higher excitation. This can be explained, for the Balmer lines, by the increase in continuum emission at the inner disc for shorter wavelengths.

A set of dotted lines in the right-hand panels indicates the slope of the empirical radial dependence of the line emissivity in accretion discs, $I \propto R^{-1.5}$, as inferred from Doppler tomography by assuming a Keplerian distribution of velocities for the emitting gas (Marsh et al. 1990). For H$\gamma$ and He I $\lambda$5876, the net emission occurs for a narrow range of radii, making a comparison with the empirical law difficult. The derived radial distributions for H$\alpha$ and H$\beta$ are clearly different from the empirical $I \propto R^{-1.5}$ law; in particular, the H$\alpha$ distribution is flat at inner and intermediate disc radii ($R < 0.3R_{L1}$). This remark suggests that the line-emitting regions on the disc surface are not in Keplerian orbits, or that a

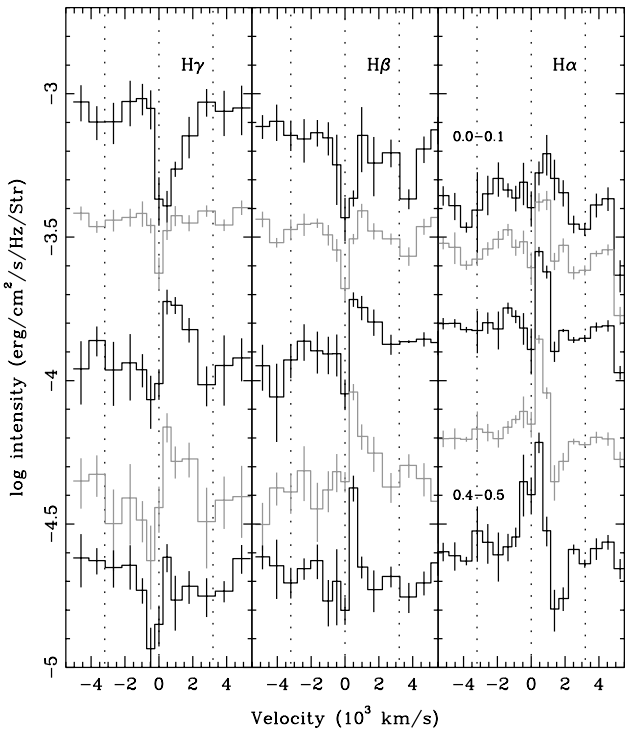


**Figure 9.** Spatially resolved spectra in the H$\alpha$, H$\beta$ and H$\gamma$ regions as a function of velocity. The notation is the same as in Fig. 8. Dotted vertical lines mark line centre and the maximum blueshift/redshift velocity expected for gas in Keplerian orbits around a 0.67-$M_\odot$ white dwarf seen at an inclination of $i = 78°$ ($v \sin i = 3200\,\mathrm{km\,s^{-1}}$).

substantial fraction of the emission lines does not arise from the accretion disc, in accordance with the inferences drawn by the comparison of velocity-resolved eclipse maps in Section 4.1. The latter hypothesis is consistent with the significant uneclipsed components inferred for the Balmer and He I lines (Section 4.4.2).

### 4.4 Spatially resolved spectra

Each of the eclipse maps yields spatially resolved information about the emitting region in a specific wavelength range. By combining all narrow-band eclipse maps, we are able to isolate the spectrum of the eclipsed region at any desired position (e.g. Rutten et al. 1994; Baptista et al. 1998).

To investigate the possible influence of the gas stream on the disc emission, and motivated by the observed asymmetries in the eclipse maps shown in Section 4.1, we divided the disc into two major azimuthal regions to extract spatially resolved spectra: the gas stream region (upper right quadrant in the eclipse maps of Figs 3 and 4) and the disc region (the remaining three-quarters of the eclipse map). For each of these regions, we divided the maps into a set of six concentric annuli centred on the white dwarf, of width $0.1R_{\rm L1}$ and with radius increasing in steps of $0.1R_{\rm L1}$. Each spectrum was obtained by averaging the intensity of all pixels inside the corresponding annulus, and the statistical uncertainties affecting the average intensities were estimated with the Monte Carlo procedure described in Section 3.2.

#### *4.4.1 Disc spectra*

Fig. 8 shows spatially resolved spectra of the disc region on a logarithmic scale. The inner annular region is at the top, and each spectrum is at its true intensity level. The spectrum of the uneclipsed component is shown in the lower panel, and will be discussed in detail in Section 4.4.2. The spectrum of the inner disc is characterized by a blue and bright continuum filled with deep and narrow absorption lines. The continuum emission becomes progressively fainter and redder for increasing disc radius, while the lines transition from absorption to emission, showing clear P Cygni profiles on all lines mapped at higher spectral resolution. The Balmer jump appears in absorption in the inner disc, and weakly in emission in the intermediate and outer disc regions, suggesting that the outer disc in UU Aqr is optically thin. The change in the slope and intensity of the continuum with increasing disc radius reflects the temperature gradient in the accretion disc, with the effective temperature decreasing outwards.

The spatially resolved spectra of the disc are plotted in Fig. 9 as a function of velocity for the H$\alpha$, H$\beta$ and H$\gamma$ regions. Vertical dotted lines mark line centre, and the maximum blueshift/redshift velocity expected for gas in Keplerian orbits around a 0.67-$M_\odot$ white dwarf as seen from an inclination of $i = 78^\circ$ ($v \sin i = 3200\,{\rm km\,s^{-1}}$) (BSC94). The absorption lines at disc centre are perceptibly narrower than expected for emission either from the white dwarf atmosphere or from disc gas in Keplerian orbits around the white dwarf. The discrepancy increases if the larger mass estimates of Diaz & Steiner (1991) and Kaitchuck et al. (1998) are assumed for the white dwarf. Moreover, the absorption lines at disc centre are deep, while lines produced in a white dwarf atmosphere or innermost disc regions should be broad and shallow. The width of the lines indicates a velocity dispersion of $\simeq 1500\,{\rm km\,s^{-1}}$ for the line-emitting region in the line of sight to

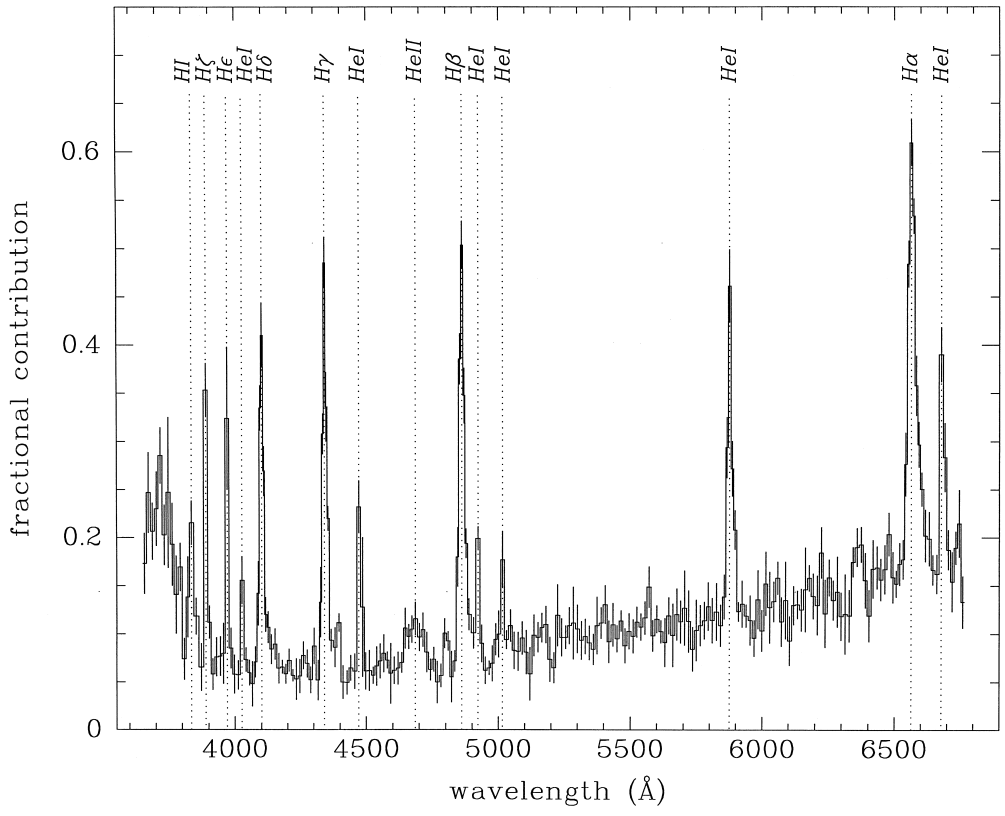


**Figure 10.** Fractional contribution of the uneclipsed component to the total flux as a function of wavelength. The values were obtained by dividing the flux of the uneclipsed component by the average out-of-eclipse level for each passband.

the disc centre, and higher velocities ($\simeq$2000 km s$^{-1}$) for the gas in the outer disc at $R \simeq 0.5R_{\rm L1}$. This is in clear disagreement with the expected behaviour of line emission from gas in a Keplerian disc, and provides additional evidence that these lines do not arise from the disc atmosphere. On the other hand, the lines at intermediate and outer disc regions ($R \gtrsim 0.2R_{\rm L1}$) show clear P Cygni profiles, indicating origin in an outflowing gas, probably the disc wind.

We note that the H$\alpha$ line shows a redshifted ($v \sim 1800$ km s$^{-1}$) absorption component in spectra of the outer disc region ($R > 0.3R_{\rm L1}$). Comparison of disc spectra at different azimuths shows that this absorption is produced in the front side of the disc, but an origin in the gas stream can possibly be ruled out since the absorption component is seen with similar strengths in the leading and trailing (the one containing the gas stream) quadrants. The interpretation of this feature is not straightforward and deserves some caution, since it is not clearly seen in any other line, and also because the surface brightness in the corresponding disc region is only a few per cent of the intensities in the inner disc.

### 4.4.2 *The uneclipsed spectrum*

The spectrum of the uneclipsed light (lower panel of Fig. 8) shows prominent Balmer and He I emission lines. The Balmer jump is clearly in emission and the optical continuum rises towards longer wavelengths, suggesting that the Paschen jump is also in emission. These results are consistent with the findings of BSH96, and indicate that the uneclipsed light has an important contribution from optically thin gas from outside the orbital plane. The Balmer lines mapped at higher spectral resolution show broad asymmetric profiles, with line peaks displaced to the red side and wings extending up to $\simeq$1500 km s$^{-1}$. The observed asymmetry is consistent with that previously seen in the integrated spectra of Diaz & Steiner (1991) and Hessman (1990), and is similar to that observed in the resonant ultraviolet lines of UX UMa, where the uneclipsed component was attributed to emission in a vertically extended disc wind (Baptista et al. 1995, 1998; Knigge & Drew 1997).

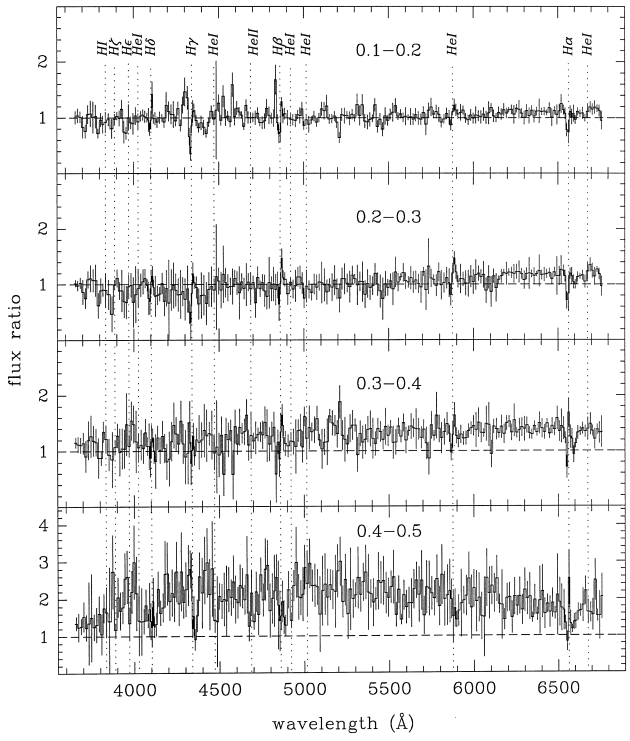


**Figure 11.** Ratio of the gas stream spectrum and the disc spectrum for the same set of annular regions as Fig. 8. Dashed lines mark the unity level for each panel. The notation is the same as in Fig. 8.

The fractional contribution of the uneclipsed component to the total flux was obtained by dividing the flux of the uneclipsed light by the average out-of-eclipse level at each passband. The result is shown in Fig. 10. The fractional contribution of the uneclipsed light is very significant for the optical emission lines, reaching 40–60 per cent at the Balmer lines and 20–40 per cent at the He I lines, and decreases steadily along the Balmer series. The difference in fractional contribution between the Balmer and He I lines and among the Balmer lines indicates the existence of a vertical temperature gradient in the material above/below the disc, with the He I lines (which require higher excitation energies) being produced closer to the orbital plane. In any case, a substantial fraction of the light at these lines does not arise from the orbital plane, and is not occulted during eclipse. The unclipsed component gives a significant contribution also to the continuum emission. About 20 per cent of the flux at the Balmer continuum and a similar fraction of the continuum emission at the red end of the spectrum arise from regions outside the orbital plane.

### 4.4.3 *The gas stream region*

Fig. 11 shows the ratio between the spectra of the gas stream region and the disc region at the same radius, as a function of radius. A dashed line marks the unity level for each panel. The comparison shows that the spectrum of the gas stream is noticeably different from the disc spectrum in the outer disc regions (where one expects a bright-spot to form, owing to the shock between the inflowing stream and the outer disc rim), but also reveals systematic differences between stream and disc spectra for a range of radii. In all cases, the stream emission is stronger than that of the adjacent disc.

This result suggests that the material in the gas stream continues to flow downstream beyond the bright-spot position. In this regard, there are three potential cases: (1) stream overflow that arcs high above/below the disc until it hits the disc surface again at a downstream position closer to the white dwarf (hereafter called the 'classical stream overflow'); (2) stream overflow that continuously skims the disc surface (hereafter called the 'disc-skimming overflow'); and (3) a stream that drills into the disc at the impact site (hereafter named the 'disc stream penetration'). The latter case seems physically unrealistic, and is not supported by hydrodynamic calculations of stream–disc interaction (Armitage & Livio 1996, 1998). The fact that there is enhanced emission in the stream region extending all the way from the outer disc down to $R \simeq 0.2R_{\rm L1}$ argues in favour of an interpretation in terms of disc-skimming overflow instead of the classical stream overflow – as has been suggested to explain the behaviour of SW Sex stars (Hellier & Robinson 1994; Hellier 1996) – since the latter would produce enhanced emission only at the position of the two spots, at the initial impact site in the outer disc edge and at the re-impact site much closer to disc centre (Lubow 1989).

The spectrum of the ratio becomes redder for decreasing disc radius, possibly a combination of the disc emission becoming bluer as one moves inwards and the gas stream emission becoming redder while its energy is continuously lost in the shock with disc material along the inward stream trajectory. This is reminiscent of

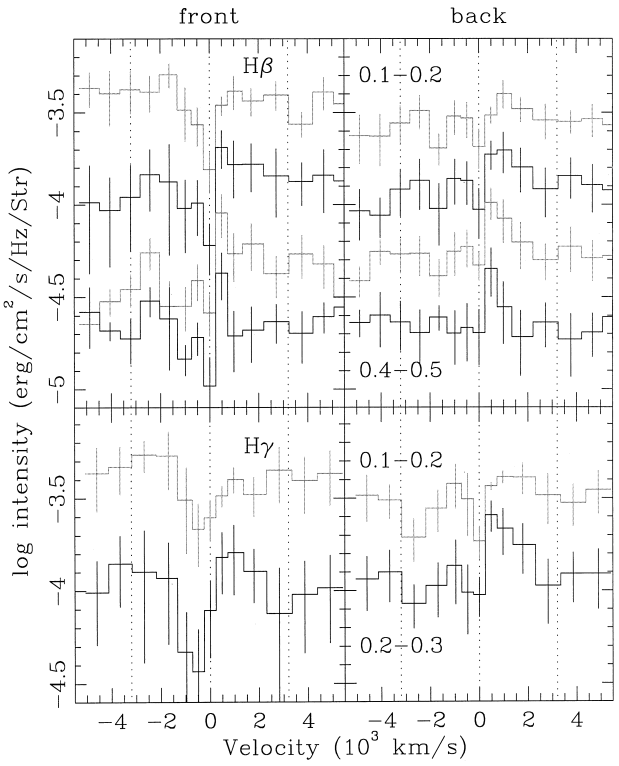


**Figure 12.** Comparison of spatially resolved spectra of the front and back sides of the disc (see text) in the H$\beta$ and H$\gamma$ regions. The notation is the same as in Fig. 9. For clarity, only the H$\gamma$ spectra of two annuli are shown.

what was seen in ultraviolet eclipse observations of the dwarf nova IP Peg in quiescence, which revealed a compact blue bright-spot with an extended red tail (Baptista et al. 1993).

## 5 DISCUSSION

In this section we present and discuss some possible interpretations for the results of Section 4 in the context of the current models for the SW Sex stars.

### 5.1 Where do the lines come from?

In previous sections we have accumulated evidence that the behaviour of the UU Aqr lines in its high state is not consistent with emission in a disc atmosphere, namely: (i) negligible rotational disturbance; (ii) no mirror symmetry between eclipse maps in symmetric velocity bins; (iii) an H$\alpha$ line emission distribution that is much flatter than the empirical $I \propto R^{-1.5}$ law; (iv) significant uneclipsed components; and (v) the presence of P Cygni profiles in the disc spectra at intermediate and large disc radii. If the lines do not arise in the disc atmosphere, where do they come from?

The most compelling interpretation is that the lines are produced in a disc chromosphere + wind. This region is hot, dense and opaque, and has low expansion velocities close to the orbital plane in order to produce the observed deep, narrow absorption lines in the line of sight to the inner disc. Most of the high-excitation lines are produced close to the disc plane. The density and temperature decrease with height above/below the disc as the outflowing gas spreads over an increasing surface area. Optically thin emission from this extended region is probably responsible for the Balmer jump (and lines) in emission observed in the uneclipsed spectrum. Support in favour of this scenario comes from the recent detailed modelling of the C IV wind line of eclipsing nova-like stars by Schlosman, Vitello & Mauche (1996) and Knigge & Drew (1997). Their results suggest the existence of a relatively dense ($n_e \sim 4 \times 10^{12}\,\mathrm{cm}^{-3}$) and vertically extended chromosphere between the disc surface and the fast-moving parts of the wind, which could produce significant amounts of optically thin emission. At orbital phases around eclipse, gas outflowing in the direction of the secondary star will be seen along the line of sight to the bright underlying accretion disc as blueshifted absorption features, while gas expelled in the direction away from the secondary star should contribute with redshifted emission.

We have tested this scenario by comparing spatially resolved spectra of the disc lune closest to the secondary star (the right hemisphere of the disc in the eclipse maps of Fig. 3, hereafter called the 'front' side) and of the disc lune farthest away from the secondary star (the left hemisphere of the disc in Fig. 3, hereafter called the 'back' side). For this purpose, we defined two opposite azimuthal disc regions of width 30° along the major axis of the binary, and extracted spatially resolved spectra for the same set of annuli as above. These spatially resolved spectra are noisier than those of Figs 8 and 9 because in this case the average intensity of each annulus is computed from a significantly smaller number of pixels. The results are shown in Fig. 12 for the H$\beta$ and H$\gamma$ regions, and are consistent with our interpretation: the blueshifted absorption component is seen mainly in the front side of the disc, while the redshifted emission is generally more prominent in spectra of the back side of the disc. The fact that the blueshifted absorption can still be seen projected along the line of sight at the outer regions of the disc favours a more spherical or equatorial geometry for the outflowing gas, instead of a highly collimated, polar jet.

The chromosphere + disc wind interpretation satisfactorily accounts for all the features listed above and also gives a plausible explanation for (1) the distinct semi-amplitude of the radial velocity $K$ and systemic velocity $\gamma$ as inferred from different emission lines, and (2) the time-dependent $K$- and $\gamma$-values (Hoard et al. 1998). The centroid of lines of different excitation level will occur at different locations in the primary lobe and will sample different velocities along the line of sight. With respect to (2), the comparison of the H$\alpha$ map of BSH96 (which corresponds to the low-brightness state) with that of Fig. 4 (the high state) reveals that in the latter the emission extends over a much larger region of the primary lobe with a pronounced asymmetry in the stream region, suggesting that the wind emission is variable in time and is intimately connected with the mass accretion rate. This remark gives additional support to the suggestion by Hoard et al. (1998) that the observed time dependence of the $K$ and $\gamma$ velocities might be due to variability of a wind component in UU Aqr.

An alternative possibility is to consider the deep absorption lines seen towards the line of sight to the disc centre as being produced by absorption in a vertically extended disc rim. Although this scenario accounts for the narrow absorption lines, it is not able to explain the large velocities inferred from the linewidth for intermediate and large disc radii, nor the P Cygni profiles. Furthermore, it should result in a perceptible front–back asymmetry in the disc surface brightness (namely, the back side of the disc should be brighter) which is not seen in the eclipse maps.

Recently, Horne (1999) proposed that most of the features of the SW Sex stars could be explained in terms of a disc-anchored magnetic propeller, in which energy and angular momentum are extracted from the magnetic field of the inner disc regions to fling part of the material in the gas stream out of the binary towards the back side of the disc. Although this model is able to explain many of the observed features of UU Aqr, it can only account for the observed P Cygni profiles if the gas trapped by the inner disc magnetic field is expelled in all directions and not only towards the back of the disc. We note that, in this case, there is no significant difference between the propeller and the disc wind models and, in fact, the former could possibly work as the underlying physical mechanism driving the latter.

If disc-skimming overflow does occur, we might expect that dissipation of energy in the collision between the gas stream and the disc material gives rise to a bulge extending along the stream trajectory over and under the disc. This bulge will appear in front of the chromosphere + wind line-emitting region at the inner disc when seen along the line of sight at orbital phases 0.5–0.9. This may explain the phase-dependent absorption lines, observed from phases 0.5 to 0.9 and with maximum at phase ~0.8 (Haefner 1989; Hoard et al. 1998). The enhanced line emission along the gas stream (see Fig. 4) is possibly responsible for the phase offset between photometric and spectroscopic conjunction (Diaz & Steiner 1991; Hoard et al. 1998).

In summary, the picture that emerges from our results is consistent with the results from the Doppler tomography and the model proposed for UU Aqr by Hoard et al. (1998).

### 5.2 Where has the bright-spot gone?

Although our observations correspond to the high-brightness state of UU Aqr, our eclipse maps do not show the conspicuous asymmetric structure seen in the high-state eclipse maps of BSH96 and which was interpreted as being the bright-spot. The explanation for the 'disappearance' of the bright-spot may be connected with the stunted outbursts found by Honeycutt et al. (1998).

BSH96 pointed out that the inferred accretion rate of UU Aqr is close to the critical mass accretion rate for disc instability to occur, and remarked that the long-term light curves of accretion discs with mass transfer rates near their critical limit might display low-amplitude ($\lesssim$1.0 mag) outbursts caused by thermal instabilities in the outer disc regions (e.g. Lin, Papaloizou & Faulkner 1985). In this case the outburst is restricted to the outer one-third of the disc extent, while the inner disc remains in a high-viscosity, steady state. Honeycutt et al. (1998) suggested that such dwarf nova type instabilities could be an explanation for the stunted outbursts of UU Aqr if a mechanism can be identified to make the amplitudes appear small. We note that the observed low amplitudes can be easily accounted for by the reduced contrast of the light from the outbursting outer regions – where the efficiency in transforming gravitational potential energy in radiation is relatively low – in comparison with the bright, optically thick and steady inner disc.

If the observed stunted outbursts of UU Aqr are caused by thermal instabilities in its outer disc, the disc radius is expected to increase during the outburst and will eventually reach the 3:1 tidal resonance radius leading to an elliptical precessing disc reminiscent of what possibly happens in SU UMa stars in superoutburst (e.g. Warner 1995 and references therein). We suggest that the azimuthally elongated structure seen in the eclipse maps of BSH96 is the signature of such an elliptical disc, and not the bright-spot. Following this line of reasoning, this structure should not be present when the disc radius is smaller than the tidal resonance radius. Support for this interpretation comes from the comparison of disc radii in the high-state eclipse maps of BSH96 and our eclipse maps. From the data of BSH96 we estimate a disc radius of $R_{\rm d} \simeq 0.7R_{\rm L1}$, comparable to the 3:1 tidal resonance radius for a mass ratio of $q = 0.3$. Our eclipse maps lead to a smaller value of $R_{\rm d} = 0.65R_{\rm L1}$. We therefore suggest that UU Aqr was in an occasional 'superhumper' state during the high brightness state observations of BSC94.

In the model of Hoard et al. (1998), after the explosive impact of the high-$\dot{M}$ accretion stream with the edge of the disc, the incoming gas forms an optically thick absorbing bulge on the disc that either follows roughly the stream trajectory or runs along the rim of the disc, producing the absorption features seen at phases 0.4–0.9. It may alternatively be possible that the structure seen in the eclipse maps of BSH96 is the signature of such post-impact stream material running along the edge of the disc. In this scenario, the azimuthally extended bulge would be present or not, depending on the (variable) mass accretion rate, and the resulting orbital hump would remain fixed in phase.

It would be interesting (although outside the scope of this paper) to re-analyse the data of BSC94 to see if the orbital hump present in the high state precesses in phase in a similar manner to superhumps in superoutbursts (supporting the elliptical disc scenario), or if its maximum occurs always at the same orbital phase range about 0.8–0.9 cycle (favouring the post-impact bulge scenario).

## 6 CONCLUSIONS

We have used time-resolved spectroscopy to study the structure and spectra of the accretion disc and gas stream of the nova-like UU Aquarii in the optical range. The main results of this analysis can be summarized as follows.

(i) The spectrum of the inner disc shows a blue continuum filled with deep, narrow absorption lines which transition to emission with clear P Cygni profiles at intermediate and large radii ($R \gtrsim 0.2R_{\rm L1}$).

(ii) The spectrum of the uneclipsed light has strong H I and He I emission lines and a Balmer jump in emission, indicating a significant contribution from optically thin regions outside the orbital plane.

(iii) Velocity-resolved eclipse maps and spectra indicate that most of the line emission probably arises in a vertically extended disc chromosphere + wind.

(iv) Differences in fractional contribution among emission lines suggest a vertical temperature gradient in the material above/below the disc.

(v) The comparison of the spectra of the gas stream region and the disc region at the same radius as a function of radius gives evidence of gas stream disc-skimming overflow down to $R \simeq 0.2R_{\rm L1}$. This may explain the phase-dependent absorption in emission lines.

(vi) The comparison of our eclipse maps with those of BSH96 suggests that the asymmetric structure in the outer disc previously identified as the bright-spot may be the signature of an elliptical disc similar to those possibly present in SU UMa stars during superoutbursts.

## ACKNOWLEDGMENTS

We gratefully acknowledge the director of KPNO for granting

telescope time for this project in the Summer Queue Program, Tod Boroson and the team of observers at KPNO for their kind efforts in collecting the data, Knox Long and the director of STScI for financial support through the Director Discretionary fund, Susan Keener for helping with the data reduction at STScI, and an anonymous referee for valuable comments and suggestions that helped to improve the presentation of the results. RB acknowledges financial support from CNPq/Brazil through grant No. 300 354/96-7. This work was partially supported by PRONEX grant FAURGS/FINEP 7697.1003.00.

## REFERENCES

Armitage P. J., Livio M., 1996, ApJ, 470, 1024
Armitage P. J., Livio M., 1998, ApJ, 493, 898
Baptista R., Steiner J. E., 1993, A&A, 277, 331
Baptista R. et al., 1993, in Shafter A., ed., ASP Conf. Ser. Vol. 56, Interacting Binary Stars. Astron. Soc. Pac., San Francisco, p. 259
Baptista R., Steiner J. E., Cieslinski D., 1994, ApJ, 433, 332 (BSC94)
Baptista R., Horne K., Hilditch R., Mason K. O., Drew J. E., 1995, ApJ, 448, 395
Baptista R., Steiner J. E., Horne K., 1996, MNRAS, 282, 99 (BSH96)
Baptista R., Horne K., Wade R. A., Hubeny I., Long K. S., Rutten R. G. M., 1998, MNRAS, 298, 1079
Diaz M. P., Steiner J. E., 1991, AJ, 102, 1417
Downes R. A., Keyes C. D., 1988, AJ, 96, 777
Haefner R., 1989, Inf. Bull. Variable Stars, 3397
Hellier C., 1996, ApJ, 471, 949
Hellier C., 2000, in Charles P. et al., eds, Cataclysmic Variables: a 60th Birthday Symposium in Honour of Brian Warner. New Astron. Rev., Elsevier, in press (astro-ph/9906089)
Hellier C., Robinson E. L., 1994, ApJ, 431, L107
Hessman F. V., 1990, in Klare G., ed., Reviews in Modern Astrophysics: Accretion and Winds. Springer, Berlin, p. 32
Hoard D. W., Still M. D., Skzody P., Smith R. C., Buckley D. A. H., 1998, MNRAS, 294, 689
Honeycutt R. K., Schlegel E. M., Kaitchuck R. H., 1986, ApJ, 302, 388
Honeycutt R. K., Robertson J. W., Turner G. W., 1998, AJ, 115, 2527
Horne K., 1985, MNRAS, 213, 129
Horne K., 1986, PASP, 98, 609
Horne K., 1993, in Wheeler J. C., ed., Accretion Disks in Compact Stellar Systems. World Scientific, Singapore, p. 117
Horne K., 1999, in Mukai K., Hellier C., eds, ASP Conf. Ser. Vol. 157, Magnetic Cataclysmic Variables. Astron. Soc. Pac., San Francisco, p. 349
Kaitchuck R. H., Schlegel E. M., White J. C., II, Mansperger C. S., 1998, ApJ, 499, 444
Knigge C., Drew J. E., 1997, ApJ, 486, 445
Lin D. N. C., Papaloizou J., Faulkner J., 1985, MNRAS, 212, 105
Lubow S. H., 1989, ApJ, 340, 1064
Marsh T. R., Horne K., Schlegel E. M., Honeycutt K., Kaitchuck R. H., 1990, ApJ, 364, 637
Massey P., Storbel K., Barnes J. V., Anderson E., 1988, ApJ, 328, 315
Rutten R. G. M., van Paradijs J., Tinbergen J., 1992, A&A, 260, 213
Rutten R. G. M., Dhillon V. S., Horne K., Kuulkers E., 1994, A&A, 283, 441
Schlosman I., Vitello P. A. J., Mauche C. W., 1996, ApJ, 461, 377
Thorstensen J. R., Ringwald F. A., Wade R. A., Schmidt G. D., Norsworthy J. E., 1991, AJ, 102, 272
Warner B., 1995, Cataclysmic Variable Stars. Cambridge Univ. Press, Cambridge
Warner B., 1997, in Wickramasinghe D. T., Bicknell G. V., Ferrario L., eds, ASP Conf. Ser. Vol. 121, Proc. IAU Colloq. 163, Accretion Phenomena and Related Outflow. Astron. Soc. Pac., San Francisco, p. 133
Williams R. E., 1989, AJ, 97, 1752